AIChE

A Gaussian Quadrature Method for Solving Batch Crystallization Models

Shamsul Qamar
Max Planck Institute for Dynamics of Complex Technical Systems Magdeburg, 39106 Germany; and Dept. of Mathematics, COMSATS Institute of Information Technology, Islamabad, Pakistan

Safyan Mukhtar and Qasim Ali
Dept. of Mathematics, COMSATS Institute of Information Technology, Islamabad, Pakistan

Andreas Seidel-Morgenstern
Max Planck Institute for Dynamics of Complex Technical Systems Magdeburg, 39106 Germany

DOI 10.1002/aic.12264
Published online April 28, 2010 in Wiley Online Library (wileyonlinelibrary.com).

The quadrature method of moments (QMOM) has been recently introduced for solving population balance models. In this article, an alternative approach of QMOM is proposed for solving batch crystallization models describing crystals nucleation, size-dependent growth, aggregation, breakage, and dissolution of small nuclei below certain critical size. In this technique, orthogonal polynomials, obtained from the lower order moments, are used to find the quadrature abscissas (points) and weights. Several test problems with different combinations of processes are considered in this manuscript. The numerical results are compared with analytical solutions and with the finite-volume scheme results. Excellent agreements were observed on the moment calculations in all test cases. © 2010 American Institute of Chemical Engineers *AIChE J,* 57: 149–159, 2011
Keywords: crystallization, particulate flows, numerical solutions, crystal growth, nucleation

Introduction

Crystallization from a solution is an important industrial operation due to marketing a large number of materials as crystalline particles. It is therefore one of the most widely used separating and purifying technique in chemical, pharmaceutical, semiconductor, and food industries. To improve the quality of a product, it is necessary to understand the kinetics of the crystallization process and the impact of process variables on the process. The desired goals can be achieved by modeling the underlying processes and by developing advanced control algorithms that can be used to optimize the resulting crystal size distributions (CSDs).

Population balance models (PBMs) have been widely used for modeling crystallization processes since the mid-1960s.[1,2] Currently, PBMs are used to model a wide range of particulate processes including comminution, crystallization, granulation, flocculation, combustion, and polymerization. Generally, the models used refer to dispersed systems that include both external (spatial) and internal (property) coordinates. The major phenomena influencing these processes include growth, nucleation, aggregation, breakage, dissolution, and inlet and outlet streams. Several numerical methods have been developed for solving population balance equations (PBEs), such as the method of moments,[1,3–6] the method of characteristics,[7,8] the method of weighted residual or orthogonal collocation,[9] the Monte Carlo simulation,[10,11] the finite difference schemes/discrete population balances,[12] the spectral methods,[13–15] and the high-resolution finite volume methods.[8,16,17]

It has been observed, that many physical and optical properties of aerosol and clouds can be estimated directly from the knowledge of lower order moments of the radial size

Correspondence concerning this article should be addressed to S. Qamar at qamar@mpi-magdeburg.mpg.de.

distribution instead of the distribution itself.[6,18] Complicated phenomena, such as nucleation, growth, and transport, contributes to the shape of aerosol size distribution. These phenomena are difficult to incorporate in the models describing aerosol in multidimensional environments, for instance models of atmospheric transport and turbulent jet flows. The modeling of size distribution not only possesses numerical difficulties but also contain more information than actually required. Hence, the method of moments is a good alternative in such situations. Generally, it is suitable in the situations where PBM is combined with the Computational Fluid Dynamics (CFD) codes.[18,19] In such problems, the external features like turbulent flow properties play an important role and hence the distribution is a function of both internal and external coordinates, leading to a large computational time. In such cases, the moments of internal coordinates converts the given PBE to transport equations that can be efficiently incorporated in the given CFD code.

The main advantage of the quadrature method of moments (QMOM) method is their low computational cost. However, no information about the particle size distribution (PSD) is available. Instead, only finite number of moments associated with the real distribution are numerically determined which may not be sufficient in special applications to judge the quality of the product. Therefore, after having computed moments, it is sometimes necessary to reconstruct the final PSD in a best possible manner. Several techniques have been reported in the literature for reconstructing PSD from finite number of available moments.[20] Moreover, discussions about the merits and demerits of different QMOM are also available in the literature.[13,21]

The solution of PBMs by using method of moments has been introduced by Hulburt and Katz[1] which is given in terms of the moments of the PSD. Different methods have been proposed for solving the closure problem raised by Hulburt and Katz[1] and are thoroughly discussed by Diemer and Olson.[22] The QMOM was first proposed by McGraw et al.[6] for modeling aerosol evolution. This promising method is based on the solution of the integrals involving the PSD through a quadrature approximation. In this method, the product difference (PD) algorithm[23] is used for finding the quadrature abscissas and weights. The method was then extended to aggregation and coagulation problems for bivariate PSD.[19,24,25] Moreover, Barrett and Webb[26] have compared the method with other available approaches, such as Laguerre quadrature approximation and the finite element method, for the solution of the aerosol general dynamic equation. Afterwards, the QMOM method has been extended for simultaneous aggregation and breakage problems.[5] Moreover, Fan et al.[27] have proposed the direct quadrature method of moments (DQMOM) as an alternative to the PD algorithm for finding the quadrature points and weights. This method tracks directly the variables appearing in the quadrature approximation, by solving the convection equation for quadrature abscissas and weights. Later on, the DQMOM was further improved by introducing an adaptive factor in the moment equations.[28] A comparison of different QMOM methods and discussion about their limitations can be found in the article by Grosch et al.[21] Recently, Gimbun et al.[29] have introduced a new QMOM method for solving the population balance equation which simultaneously solves the differential equations for the moments and the system of nonlinear equations resulting from the quadrature approximation as a differential algebraic equation system. The authors have claimed that this method provides an efficient way of calculating the quadrature abscissas and weights.

In most of the available QMOM methods, solutions are restricted to small number of moments. Although, small number of moments can be sufficient to describe certain particulate process, a larger number of moments may be needed in other applications, for example reconstruction of the particle size-distribution from moments.[20,30] In this article, an alternative QMOM method is proposed for solving batch crystallization models describing crystals nucleation, size-dependent growth, aggregation, breakage, and dissolution of small nuclei below certain critical size. In this technique, orthogonal polynomials, obtained from the lower order moments, are used to find the quadrature points and weights. To ensure a good accuracy of the scheme, a third order orthogonal polynomial, utilizing the first six moments, is chosen to calculate the quadrature points (abscissas) and corresponding quadrature weights. Therefore, we need to solve at least six-moment system, i.e., $\mu_0,\ldots,\mu_5$. This choice of polynomial gives a three-point Gaussian quadrature rule which generally yields exact results for polynomials of degree five or less. The expression for the desired orthogonal polynomial can be derived analytically and the required number of moments increases with the order of polynomial. Note that, the calculation of at least six moments are needed to construct our third order polynomial at each time time. However, the method itself is not restricted to the calculation of any specified number of moments. One can calculate further moments by just adding ordinary differential equations (ODEs) of higher order moments to the moment system. Several numerical test problems are considered in this manuscript. The numerical results of the QMOM are validated against the analytical solutions, results available in the literature, and the results of the finite-volume scheme.[8] Excellent agreements were observed in the moments calculations for all test cases.

This article is organized as follows. In Section ''General population balance model for batch crystallization'', we formulate the one-dimensional batch crystallization model for simultaneous processes. In Section ''The quadrature method of moments'', QMOM is derived. In Section ''Numerical test Problems'', numerical test problems are presented. Finally, Section ''Conclusions'' gives conclusions and remarks.

General Population Balance Model for Batch Crystallization

In this section, a mathematical model for an ideally mixed batch crystallizer equipped with a fines dissolution unit is introduced (see Figure 1). Crystallization process form a disperse system where solid phase is dispersed in the continuous medium of the liquid phase. In the framework of PBEs, the state of an individual solid crystal is represented by an internal coordinate representing crystal size. A population of crystals is characterized by its CSD, which is described mathematically by a number density function $n(t,x)$ and is a function of time t and the crystal size x. This function describes the (average) number of crystals per crystal size.

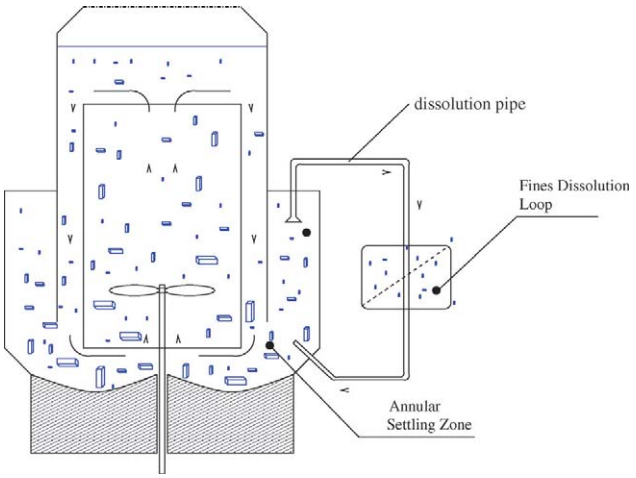

Figure 1. Single-batch process setup with fines dissolution.

[Color figure can be viewed in the online issue, which is available at wileyonlinelibrary.com.]

The rate of change in CSD is described by the population balance equation[1,2]

$$\frac{\partial n(t,x)}{\partial t} = \underbrace{-\frac{\partial[G(t,x)n(t,x)]}{\partial x}}_{\text{growth}} \underbrace{-\frac{\dot{V}}{V_c}h(x)n(t,x)}_{\text{death due to dissolution}} \underbrace{+B_0\delta(x-x_0)}_{\text{nucleation}} \underbrace{+\frac{x^2}{2}\int_0^x \frac{\beta((x^3-\lambda^3)^{1/3},\lambda)n(t,(x^3-\lambda^3)^{1/3}))n(t,\lambda)}{(x^3-\lambda^3)^{2/3}}d\lambda}_{\text{birth due to aggregation}} \underbrace{-n(t,x)\int_0^\infty \beta(x,\lambda)n(t,\lambda)d\lambda}_{\text{death due to aggregation}} + \underbrace{\int_x^\infty a(\lambda)b(x|\lambda)n(t,\lambda)d\lambda}_{\text{birth due to breakage}} \underbrace{-a(x)n(t,x)}_{\text{death due to breakage}}, \quad (1)$$

where, G represents the size-dependent growth rate, B_0 is the nucleation rate, δ is the Dirac delta function, x_0 represents the size of the nuclei, β represents the aggregation kernel, a is the breakage kernel, and b is the daughter particle size distribution. Moreover, V_c is the volume of the crystallizer, $\dot{V}$ is the volumetric flow rate from the crystallizer to the dissolution unit, and the death function $h(x)$ describes the dissolution yield of small particles below some critical size.

In addition to the solid phase, the liquid phase has to be modeled in terms of a corresponding mass balances. A balance law for the liquid phase yields an ordinary differential equation for the solute mass and accounts for the exchange of matter between the solid and the liquid phases

$$\frac{dm(t)}{dt} = \dot{m}_{in}(t) - \dot{m}_{out}(t) - 3\rho_c k_v \int_0^\infty x^2 G(t,x)n(t,x)dx, \quad (2)$$

with initial data $m(0) = m_0$. Here, ρ_c is the density of crystals and k_v is a volume shape factor defined such that the volume of a crystal with length x is $k_v x^3$. The negative sign of the last term on the right-hand side of Eq. 2 shows that solute mass in the solution decreases during crystallization. Because of the fines dissolution this equation has two mass fluxes. The first one $\dot{m}_{out}(t)$ is the mass flux in the liquid phase which is being taken out from the crystallizer to the dissolution unit (the pipe). The second one $\dot{m}_{in}(t)$ is the incoming mass flux in the crystallizer from the dissolution unit. They are defined as

$$\dot{m}_{out}(t) = w(t)\rho_{solu}(T)\dot{V}, \quad (3)$$

$$\dot{m}_{in}(t) = \dot{m}_{out}(t_d) + \frac{k_v\rho_c\dot{V}}{V_c}\int_0^\infty x^3 h(x)n(t_d,x)dx - k_v\rho_c x_0^3 B_0(t_d), \quad (4)$$

where, $t_d := t - t_p$. Here, $w(t)$ represents mass fraction which is defined as

$$w(t) = \frac{m(t)}{m(t) + m_{solv(T)}}, \quad (5)$$

where, $m_{solv}(T)$ is the mass of solvent and $\rho_{solu}(T)$ is the density of the solution, both are defending on the temperature T. The temperature T can be constant (isothermal case) or can be a decreasing function of time (nonisothermal case). Moreover, $t_p \geq 0$ represents residence time in the dissolution unit (the pipe). It is defined as

$$t_p = \frac{V_p}{\dot{V}}, \quad (6)$$

where V_p represents volume of the pipe. The above model reduces to the case of fines dissolution without time delay when $t_p = 0$. Moreover, the model reduces to the case without fines dissolution when the second last term on the right-hand side of Eq. 1 and the first two terms on the right-hand side of Eq. 2 are zero. Then, Eqs. 3 and 4 are not required.

With the moment transformation of the distribution function, the PBE in Eq. 1 can be further simplified. The kth moment is defined as

$$\mu_k(t) = \int_0^\infty x^k n(t,x)dx. \quad (7)$$

The first four moments have the following physical meanings; i.e., μ_0 is related to the total number of particles in the system, μ_1 is the total length of particles in the system, μ_2 is the total surface area of particles, and μ_3 is the total volume of particles in the system. After applying the moments transformation, our PBE (1) becomes[1,29]

$$\begin{aligned}\frac{d\mu_k(t)}{dt} =& \int_0^\infty kx^{k-1}G(t,x)n(t,x)dx - \frac{\dot{V}}{V_c}\int_0^\infty x^k h(x)n(t,x)dx + x_0^k B_0(t) \\ &+ \frac{1}{2}\int_0^\infty n(t,\lambda)\int_0^\infty \beta(u,\lambda)(u^3+\lambda^3)^{k/3}n(t,u)dud\lambda \\ &- \int_0^\infty x^k n(t,x)\int_0^\infty \beta(x,\lambda)n(t,\lambda)d\lambda dx \\ &+ \int_0^\infty x^k \int_x^\infty b(x|\lambda)a(\lambda)n(t,\lambda)d\lambda dx - \int_0^\infty x^k a(x)n(t,x)dx.\end{aligned} \quad (8)$$

Derivation of the right-hand side terms is trivial except the second term. The second term can be obtained by introducing the variable $u^3 = x^3 - \lambda^3$ and by substituting $x^2dx = u^2du$.

The first integral in above equation can be solved for size-independent growth, but not for the size-dependent growth, with the standard method of moments techniques. However, still it is not possible to solve integrals in the dissolution, aggregation, and breakage terms due to closure problem, as these integrals cannot be written in term of moments. Hence, the QMOM is needed to overcome the closure problem.

The Quadrature Method of Moments

In numerical analysis, a quadrature rule is an approximation of the definite integral of a function as a weighted sum of function values at specified points within the domain of integration. Normally, an approximation to the definite integral is calculated by summing up the functional values at a set of equally spaced points, each value multiplied by a certain weight. However, in Gaussian quadrature rule we have freedom to choose not only the weights but also the points (abscissas) at which the function is evaluated. The chosen abscissas are not necessarily equally spaced. Let, we have an integral of the form $\int_a^b \psi(x)f(x)dx$, where $\psi(x)$ denotes a nonnegative weight function and $f(x)$ is a nonspecified function of x. Then, we can find a set of weights w_i and abscissas x_i such that the approximation

$$\int_a^b \psi(x)f(x)dx \approx \sum_{i=1}^{N} w_i f(x_i) \tag{9}$$

is exact if $f(x)$ is a sufficiently smooth function. The theory behind Gaussian quadrature is based on orthogonal polynomials. To calculate a special orthogonal polynomial of order n one has to construct a set of polynomials that includes exactly one polynomial of order i for each $i = 1,2,\ldots$, where all of them are mutually orthogonal over a specified weight function $\psi(x)$.[31] This can be explained by defining the scalar product of two functions $r(x)$ and $s(x)$ over a weight function $\psi(x)$ as

$$<r|s>=\int_a^b \psi(x)r(x)s(x)dx. \tag{10}$$

Now, two functions are said to be orthogonal if their scalar product is zero. If there is no classical weight function $\psi(x)$ given, as in our case, one needs additional information to obtain the weights and abscissas. In our situation, we can use the moments

$$\mu_k(t) = \int_0^\infty x^k n(t,x)dx \approx \sum_{i=1}^{N} x_i^k w_i, \tag{11}$$

where, the $n(t,x)$ is used as weight function $\psi(x)$ and x^k is the kth order polynomial $p(x)$. We need $2N$ moments, i.e., from μ_0 to μ_{2N-1}, to calculate N pairs of weights and abscissas. It is also important to mention that the approximation is exact if $i \leq 2N-1$. For better accuracy of the scheme, we have decided to set $N = 3$. Therefore, we need to solve at least six-moment system, i.e., $\mu_0,\ldots,\mu_5$, given by Eq. 8. These six moments are needed for defining our selected third order polynomial and the required number of moments increases as the order of polynomial increases. After applying the quadrature rule (11), the integral terms in Eqs. 2 and 8 can be approximated as

$$\frac{d\mu_k(t)}{dt} = \underbrace{k\sum_{i=1}^{N} w_i x_i^{k-1} G(t,x_i)}_{\text{growth}} - \underbrace{\frac{\dot{V}}{V_c}\sum_{i=1}^{N} w_i x_i^k h(x_i)}_{\text{death due to fines dissolution}} + \underbrace{x_0^k B_0}_{\text{nucleation}}$$
$$+ \underbrace{\frac{1}{2}\sum_{i=1}^{N} w_i \sum_{j=1}^{N} w_j \beta(x_i,x_j)(x_i^3+x_j^3)^{k/3}}_{\text{birth due to aggregation}} - \underbrace{\sum_{i=1}^{N} w_i x_i^k \sum_{j=1}^{N} w_j \beta(x_i,x_j)}_{\text{death due to aggregation}}$$
$$+ \underbrace{\sum_{i=1}^{N} w_i a(x_i)\overline{b}_i^{(k)}}_{\text{birth due to breakage}} - \underbrace{\sum_{i=1}^{N} w_i a(x_i) x_i^k}_{\text{death due to breakage}}, \quad k = 0,1,2,\cdots, \tag{12}$$

$$\frac{dm(t)}{dt} = \dot{m}_{\text{in}}(t) - \dot{m}_{\text{out}}(t) - 3\rho_c k_v \sum_{i=1}^{N} w_i x_i^2 G(t,x_i), \tag{13}$$

where $\overline{b}_i^{(k)} = \int_0^\infty x^k b(x|\lambda)dx$. To obtain the quadrature points and weights in Eqs. 12 and 13, we use orthogonal polynomials. The procedure of deriving orthogonal polynomials is given below. Let us define the recursion relation

$$p_{-1} = 0, \quad p_0 = 1, \quad p_j = (x - a_j)p_{j-1} - b_j p_{j-2}, \tag{14}$$

with

$$a_j = \frac{<xp_{j-1}|p_{j-1}>}{<p_{j-1}|p_{j-1}>}, \quad j = 1,2,\cdots, \tag{15}$$

$$b_j = \frac{<p_{j-1}|p_{j-1}>}{<p_{j-2}|p_{j-2}>}, \quad j = 2,3,\cdots. \tag{16}$$

As $n(t,x)$ is used as a weight function, $\psi(x)$, therefore we get from Eq. 10

$$<p_j|p_j>=\int_a^b n(t,x)p_j^2dx. \tag{17}$$

With these definitions, we can calculate the polynomials one after another until we reach to our required nth-order polynomial. The roots of that polynomial will give us the required quadrature points x_i, for $i = 1,2,\ldots,N$. The procedure is explained below. The first order polynomial is given as

$$p_1(x) = (x - a_1)p_0 = (x - a_1). \tag{18}$$

Here, we need a_1 to get expression for p_1. This is given as

$$a_1 = \frac{<xp_0|p_0>}{<p_0|p_0>} = \frac{\int_0^\infty xn(t,x)p_0^2dx}{\int_0^\infty n(t,x)p_0^2dx} = \frac{\mu_1(t)}{\mu_0(t)}. \tag{19}$$

Thus, we have

$$p_1(x) = x - \frac{\mu_1}{\mu_0}. \tag{20}$$

Next, p_2 is given as

$$p_2 = (x - a_2)p_1 - b_2 p_0, \tag{21}$$

where according to Eqs. 15 and 20

$$a_2 = \frac{<xp_1|p_1>}{<p_1|p_1>} = \frac{\int_0^\infty xn(t,x)p_1^2 dx}{\int_0^\infty n(t,x)p_1^2 dx} = \frac{\int_0^\infty xn(t,x)\left(x - \frac{\mu_1}{\mu_0}\right)^2 dx}{\int_0^\infty n(t,x)\left(x - \frac{\mu_1}{\mu_0}\right)^2 dx} = \frac{\mu_3\mu_0^2 - 2\mu_0\mu_1\mu_2 + \mu_1^3}{\mu_2\mu_0^2 - \mu_0\mu_1^2} \tag{22}$$

and

$$b_2 = \frac{<p_1|p_1>}{<p_0|p_0>} = \frac{\int_0^\infty xn(t,x)\left(x - \frac{\mu_1}{\mu_0}\right)^2 dx}{\int_0^\infty n(t,x)dx} = \frac{\mu_2\mu_0 - \mu_1^2}{\mu_0^2}. \tag{23}$$

Hence, Eq. 21 becomes

$$p_2(x) = \frac{x^2(\mu_0\mu_2 - \mu_1^2) + x(\mu_1\mu_2 - \mu_0\mu_3) + \mu_1\mu_3 - \mu_2^2}{\mu_0\mu_2 - \mu_1^2}. \tag{24}$$

In this manner, one can calculate higher order polynomials. The third order polynomial $p_3(x)$ is given as

$$p_3(x) = x^3 + \frac{(\mu_2\mu_4\mu_1 - \mu_0\mu_4\mu_3 + \mu_2\mu_0\mu_5 + \mu_3^2\mu_1 - \mu_5\mu_1^2 - \mu_2^2\mu_3)x^2}{\mu_2^3 - \mu_2\mu_4\mu_0 - 2\mu_2\mu_3\mu_1 + \mu_3^2\mu_0 + \mu_4\mu_1^2} + \frac{(\mu_2\mu_5\mu_1 + \mu_0\mu_4^2 - \mu_0\mu_5\mu_3 - \mu_4\mu_3\mu_1 - \mu_2^2\mu_4 + \mu_2\mu_3^2)x}{\mu_2^3 - \mu_2\mu_4\mu_0 - 2\mu_2\mu_3\mu_1 + \mu_3^2\mu_0 + \mu_4\mu_1^2} + \frac{2\mu_2\mu_4\mu_3 - \mu_2^2\mu_5 - \mu_3^3 - \mu_4^2\mu_1 + \mu_5\mu_3\mu_1}{\mu_2^3 - \mu_2\mu_4\mu_0 - 2\mu_2\mu_3\mu_1 + \mu_3^2\mu_0 + \mu_4\mu_1^2}. \tag{25}$$

The roots of the selected polynomial, for example $p_3(x)$ in Eq. 25, denote the quadrature points (abscissas) x_i in Eqs. 12 and 13. After having the abscissas the next step is to calculate the quadrature weights, w_i. The expression for weights is given as[31]

$$w_i = \frac{<p_{N-1}|p_{N-1}>}{p_{N-1}(x_i)p'_N(x_i)}, \quad i = 1, 2, \cdots, N, \tag{26}$$

where, N represents the order of chosen polynomial.

Finally, the resulting system of ODEs in Eqs. 12 and 13 can be solved by any standard ODE solver. In this study, we have used the built-in Matlab subroutine *RK45*, which an embedded adaptive Range-Kutta method of order four and five.

Numerical Test Problems

In this section, several numerical test problems with different combinations of processes are considered. In the literature, several authors have solved such problems by applying variety of numerical methods.[5,8,28,29,32] For validation, we compare the numerical results of our scheme with available analytical solutions. However, in the test problems with no analytical solutions, the numerical results of our scheme are validated against the results of a high-resolution finite volume scheme.[8] In all test problems, symbols are used for the numerical results of our QMOM technique and lines are used either for analytical solutions or finite volume scheme (FVS) results.

Problem 1. Nucleation and growth with fines dissolution.

In this problem, we consider a batch crystallizer in which nucleation and growth are the dominant phenomena and is equipped with a fines dissolution unit (see Figure 1). Moreover, a time delay in the dissolution pipe is also incorporated in the model. The aggregation and breakage kinetics are neglected in this process, i.e., the last four terms on the right-hand side of Eq. 12 are absent.

The size-dependent crystal growth rate is defined as[33]

$$G(t,x) = k_g[S(t) - 1]^g(1 + \alpha_1 x)^{\alpha_2}, \tag{27}$$

where, k_g is the growth rate constant and α_1, α_2 are constants. The exponent g denotes the growth order. Moreover, $S(t)$ is the supersaturation of the dissolved component which is decreasing during the batch crystallization process. It is defined as

$$S(t) = \frac{w(t)}{w_{eq}(t)}, \tag{28}$$

where, $w_{eq}(t)$ is the equilibrium mass fraction and $w(t)$ is given by Eq. 5. The nucleation rate is given as[33]

$$B_0(t) = k_b[S(t) - 1]^b \mu_3(t), \tag{29}$$

where $\mu_3(t)$ is the third moment, k_b is nucleation rate constant and the exponent b gives the nucleation order.

The initial data are taken as[32]

$$n(0,x) = \frac{m_{seeds}}{k_v \rho_c \mu_3(0)\sqrt{2\pi\sigma_1}} \exp\left(\frac{(x - \overline{x})^2}{2\sigma^2}\right). \tag{30}$$

The minimum and maximum crystal sizes considered are $x_0 = 0$ and $x_{max} = 0.005$ m, respectively. The interval $[0, x_{max}]$ is subdivided into 300 grid points and the final simulation time in most cases is 800 min. In the case of size-dependent growth rate, we have chosen $\alpha_1 = 200\ m^{-1}$ in Eq. 27, while $\alpha_2 = 1$ in all cases. For size-independent case $\alpha_1 = 0$. The kinetic parameters and other constants are given in Table 1.

The crystallizer was kept at a constant temperature of 33°C. The following dimensionless smooth death function $h(x)$ is assumed in this problem

$$h(x) = \frac{1}{\sqrt{2\pi}\sigma_1} e^{-\left(\frac{x}{\eta_1\sigma_1}\right)^2}, \qquad \sigma_1 = \frac{1}{\sqrt{2\pi}n_{max}}, \tag{31}$$

where, $\eta_1 = 1.1547 \times 10^3$ m and $n_{max} = 0.6$.

In Figure 2, the plots of normalized moments for size-independent and size-dependent growth rates and without fines dissolution are presented. Analytical solutions are not available for this problem. Therefore, we have compared the results of our scheme with those obtained from the high-

Table 1. Parameters for the Test Problem 1

Descriptions	Symbols	Value	Units
Growth rate constant	k_g	1.37×10^{-5}	m/min
Growth rate exponent	g	0.73	–
Nucleation rate constant	k_b	3.42×10^{7}	$1/m^3$ min
Nucleation rate exponent	b	2.35	–
Density of crystals	ρ_c	1250	kg/m^3
Volume shape factor	k_v	0.029	–
Initial solute concentration (mass)	$m(0)$	0.09915	kg
Saturated mass fraction	w_{sat}	0.090681	–
Mass of seeds	m_{seeds}	2.5×10^{-3}	kg
Mass of solvent	m_{solv}	0.8017	kg
Density of solution	ρ_{solu}	1000	kg/m^3
Volume of the crystallizer	V_c	10^{-3}	m^3
Volumetric flow rate	$\dot{V}$	2×10^{-5}	m^3
Volume of the pipe	V_p	2.4×10^{-4}	min/m
Constant of initial CSD (Eq. 30)	σ	3.2×10^{-4}	m
Constant of initial CSD (Eq. 30)	$\bar{x}$	1.4×10^{-3}	m

resolution finite volume schemes of Ref. 8. Here, symbols are used for the numerical results of our QMOM technique and lines represent the finite volume scheme results. Both schemes give overlapping results. Figure 3 shows the plots of normalized moments for size-independent and size-dependent growth rates and with fines dissolution. It can be seen that, with fines dissolution the number of crystals reduces, i.e., μ_0 diminishes. However, the total volume, $\mu_3(t)$, of crystals increases. Finally, Figure 4 shows plots for the solute mass. The plots show that the solute mass improves due to fines dissolution. Table 2 gives a comparison of absolute and relative errors in the mass balances as well as CPU time in the case of size-independent growth rate. No significant changes were observed in the case of size-dependent growth rate. The observed data show that our QMOM method is efficient and preserves the mass balance. The program was written in Matlab 6.5 software under Linux operating system and was compiled on a computer

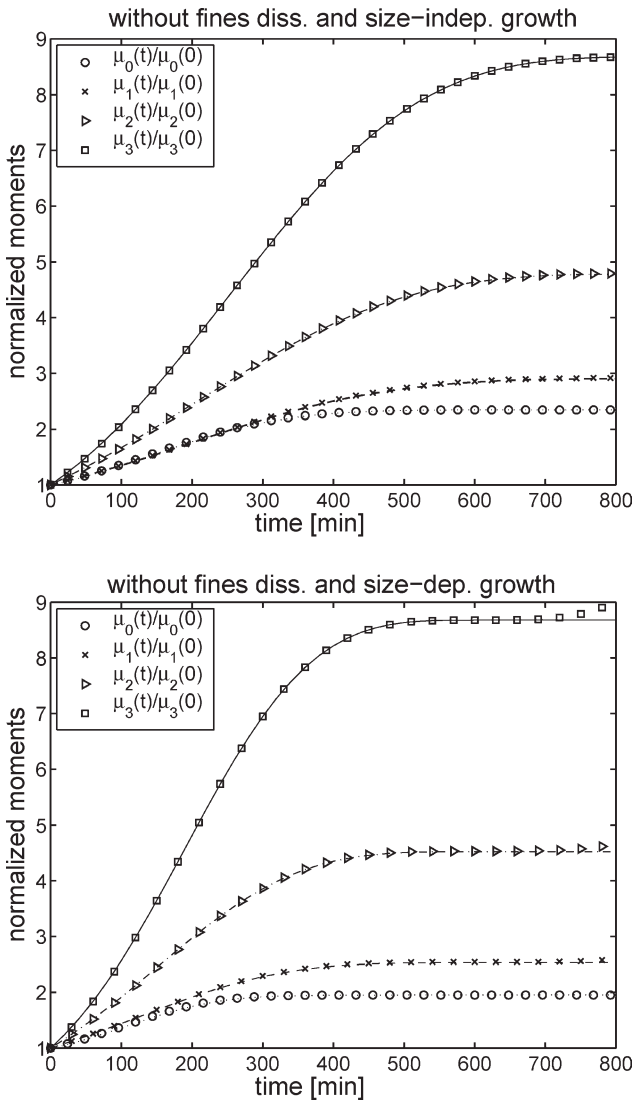

Figure 2. Problem 1: a comparison of normalized moments without fines dissolution (lines: FVS solution, symbols: QMOM solution).

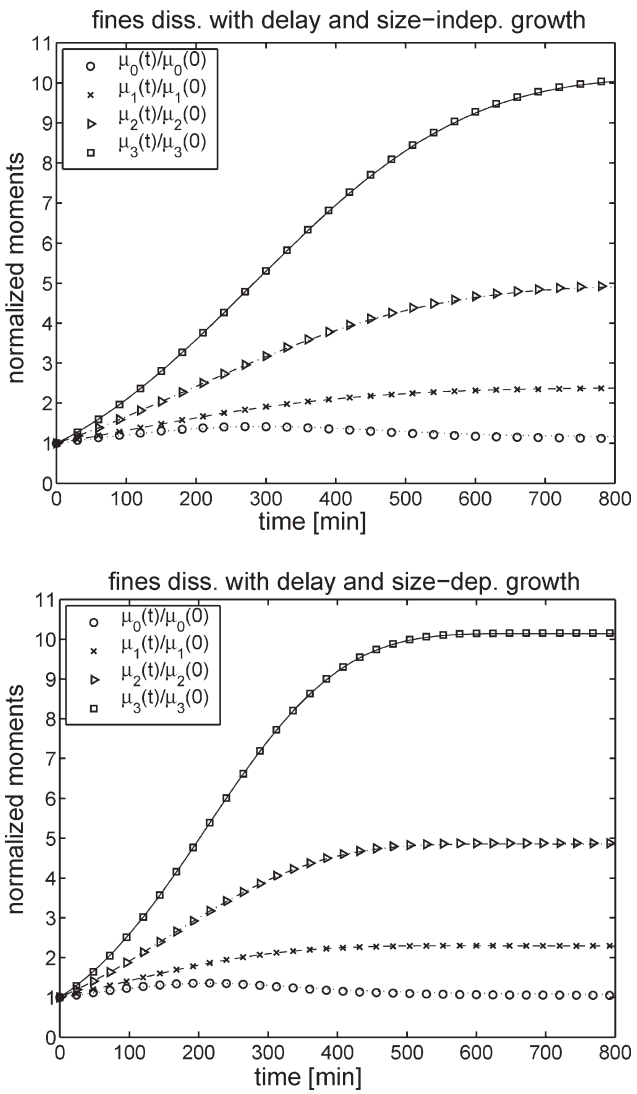

Figure 3. Problem 1: a comparison of normalized moments with fines dissolution (lines: FVS solution, symbols: QMOM solution).

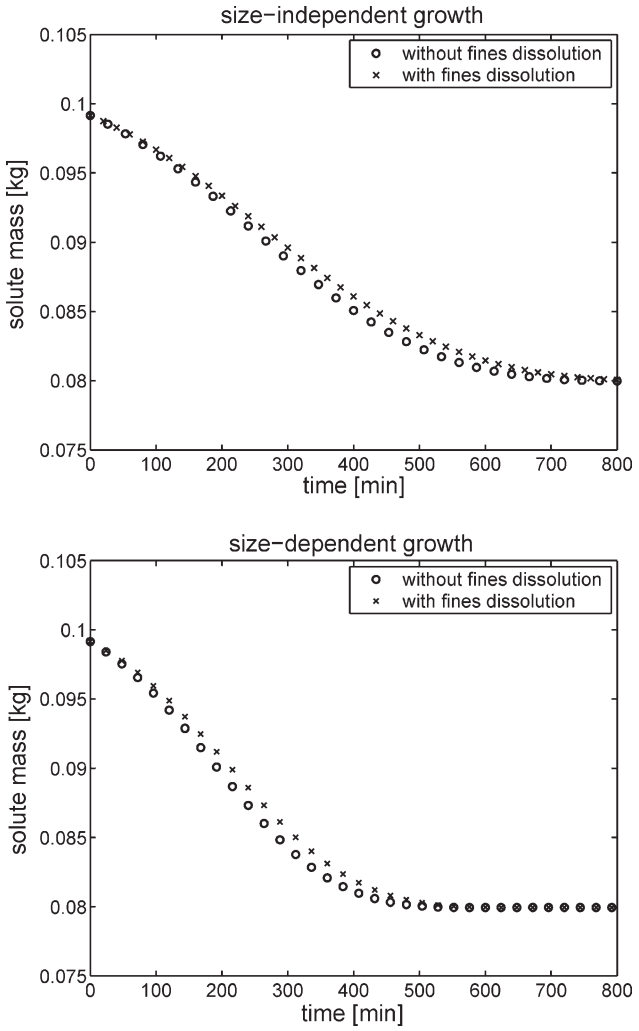

Figure 4. Problem 1: solute masses from QMOM.

with Intel(R) Core 2 Duo processor of speed 2 GHz and memory (RAM) 3.83 GB.

Problem 2. Pure aggregation.

Here, we test the performance of our numerical scheme for pure aggregation problem which takes place in various particulate processes, for example fluidized beds, formation of rain droplets, and production of dry powders. Other processes, namely breakage, growth and nucleation, give no effect throughout the course of action. Due to binary aggregation of particles, the total number of particles, $\mu_0(t)$, decreases but the total mass of the particles, $\mu_3(t)$, remains constant throughout the processing time. The following test cases are selected for describing aggregation phenomena.[28,34] Initially, at $t = 0$, the exponential particle size distribution is given by

$$n(0,x) = \frac{3N_0}{V_0}x^2 \exp\left(-\frac{x^3}{V_0}\right), \tag{32}$$

where, $N_0 = 1\ \mathrm{m}^{-3}$ and $V_0 = 1\ \mathrm{m}^3$. In the following, we consider different choices of aggregation kernel.

Case 1. Constant aggregation kernel.

In this problem, the aggregation kernel is set to be constant $\beta_0 = 1$ and is given by $\beta(x, \lambda) = \beta_0$. The analytical solution is given as[19]

$$\mu_k(t) = \mu_k(0)\left(\frac{2}{2+N_0\beta_0 t}\right)^{1-\frac{k}{3}}. \tag{33}$$

The plots in Figure 5 show normalized moments and relative errors in the numerical solutions. In the moments plot, lines are used for exact solutions and symbols are used for QMOM results. The error analysis verifies the validity of our method. In μ_0 and μ_3, the solution is approximated efficiently; the error is estimated below 10^{-7}. Here, we have not displayed relative error of μ_3. The error in first moment is $<10^{-4}$ which is further decreased up to 10^{-5} after the passage of time. It can be seen that the maximum error attained by μ_4 is below 3.5×10^{-4} which seems to be a fair approximation. The relative errors are even less than those published in the literature.[29,34]

Case 2. Sum aggregation kernel.

Next, we use a sum kernel of the form $\beta(x,\lambda) = \beta_0(x^3 + \lambda^3)$, where x and λ are the sizes of particles and $\beta_0 = 0.01$. The initial particle size distribution is the same as given by Eq. 32. The exact solution for the number density $n(t,x)$ is given by[35]

$$n(t,x) = \frac{3V_0(1-\eta)}{x\sqrt{\eta}}\exp\left(-(1+\eta)x^3/V_0\right)I_1\left(\frac{2x^3\sqrt{\eta}}{V_0}\right), \tag{34}$$

where, $\eta = 1 - \exp(-\tau)$, $\tau = \beta_0 V_0 N_0 t$, and I_1 is the modified Bessel function of first kind of order one. Figure 6 shows that the moments of our numerical scheme has a good conformity with analytical ones. It can also be observed that the maximum error occurred in μ_4 is of the order of 10^{-5} and minimum error μ_0 and μ_3 are of the order 10^{-16}. Here, we have not displayed the relative error for $\mu_3(t)$. Once again, the results of our scheme agree well with analytical solutions and even give less errors than other QMOM methods available in the literature.[29,34]

Case 3. Product aggregation kernel.

The product aggregation kernel is given by $\beta(x,\lambda) = \beta_0 x^3\lambda^3$, where $\beta_0 = 0.01$. The initial distribution is the same as given by Eq. 32. The analytical solution is given by[35]

$$n(t,x) = \frac{3N_0x^2}{V_0}\exp(-x^3(1+\tau)/V_0)\sum_{k=0}^{\infty}\left(\frac{\tau^k(x^3/V_0)^{3k}}{(k+1)!\Gamma(2k+2)}\right), \tag{35}$$

where $\tau = N_0\beta_0 V_0^2 t$ and Γ is the gamma function. The product kernel is a gelling kernel for any initial distribution, therefore

Table 2. Problem 1: Errors in Mass Balances (Size-Independent Growth)

Description	Absolute Error	Relative Error	CPU Time (s)
Without fines dissolution	1.39×10^{-7}	1.37×10^{-6}	11.6
Fines dissolution without delay	1.39×10^{-7}	1.37×10^{-6}	11.8
Fines dissolution with delay	5.8×10^{-4}	4.16×10^{-3}	15.8

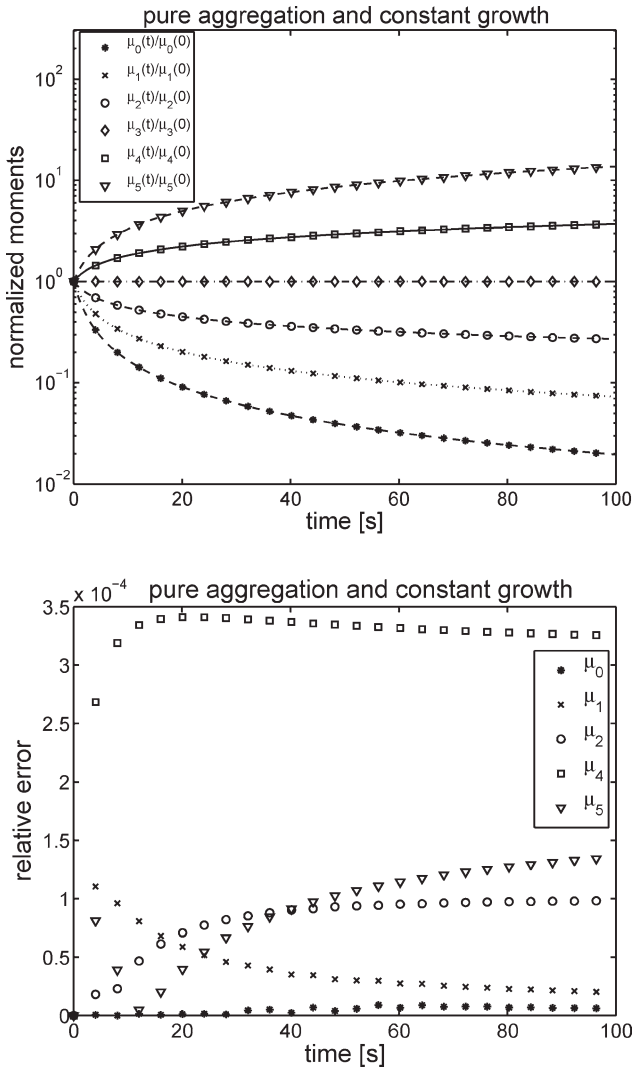

Figure 5. Problem 2 (Case 1): pure aggregation with constant kernel (lines: exact solution, symbols: QMOM solution).

the simulation was carried out before the gelling time t_{gel} arrives. The actual value for t_{gel} is given as[33,36]

$$t_{gel} = \frac{1}{\beta_0 \mu_6(0)}. \tag{36}$$

In the current test problem the gelling time was 50 *s*. The numerical results are shown in Figure 7. Both analytical and numerical results are overlapping. It was observed that μ_0 and μ_3 have relative errors upto 10^{-15} and 10^{-16}. Therefore, we have not displayed error in $\mu_3(t)$. For other moments, the maximum error is approximately up to the order of 10^{-3}. The numerical results seems pretty well as compared to those obtained by.[28,34]

Problem 3. Pure breakage.

The breakage process can be observed in several industrial applications, for example it is a dominant process in grinding mills. Due to the breakage of particles, the total number of particles increases but the total volume of the particles remains constant throughout the process.

The initial particle size distribution is the same as given by Eq. 32. A power kernel for breakage process

$$a(x) = a_0 x^3, \quad a_0 = 0.01 \tag{37}$$

and a uniform daughter distribution

$$b(x|\lambda) = \begin{cases} 6x^2/\lambda^3, & 0 < x < \lambda, \\ 0, & \text{otherwise}, \end{cases} \tag{38}$$

are considered. An analytical solution for this problem is given as[37]

$$n(t,x) = 3x^2 \frac{N_0}{V_0}(1 + C_0 V_0 t)^2 \exp\left(-\frac{x^3}{V_0}(1 + C_0 V_0 t)\right). \tag{39}$$

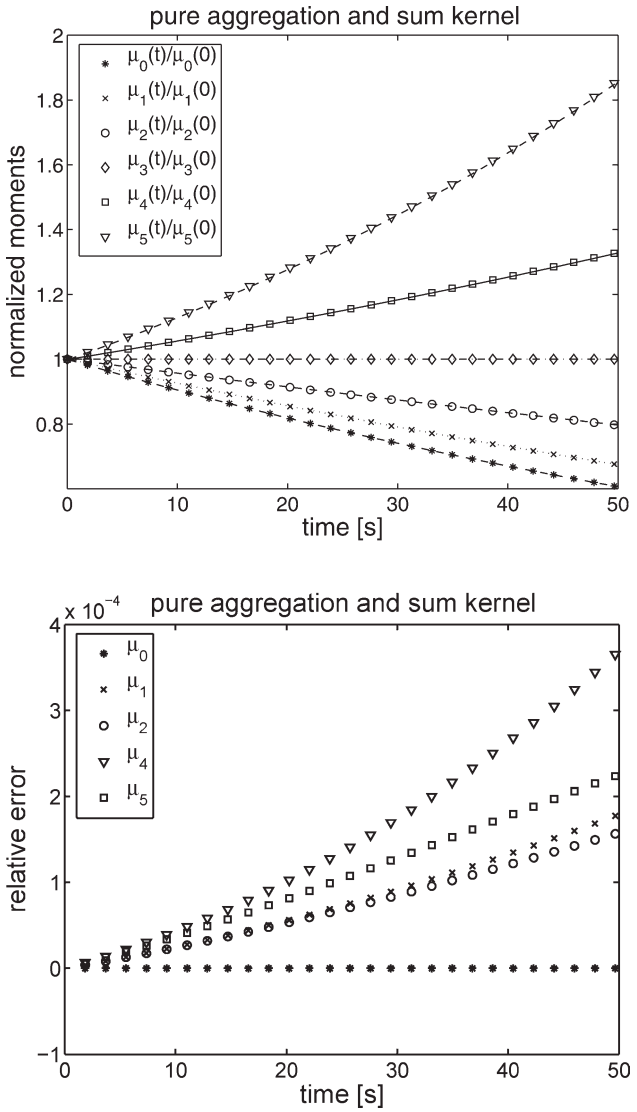

Figure 6. Problem 2 (Case 2): pure aggregation with sum kernel (lines: exact solution, symbols: QMOM solution).

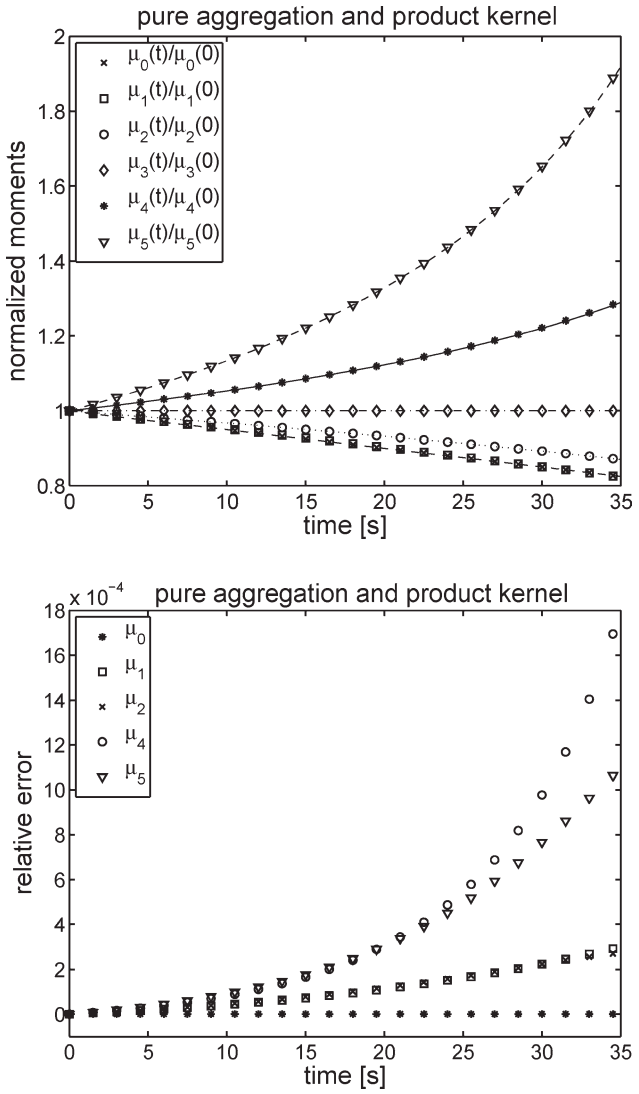

Figure 7. Problem 2 (Case 3): pure aggregation with product kernel (lines: exact solution, symbols: QMOM solution).

The numerical results are shown in Figure 8. Both analytical an numerical results are overlapping. It was observed that μ_0 and μ_3 have relative errors up to 10^{-11} and 10^{-15}. Therefore, we have not displayed error in $\mu_3(t)$. For other moments, the maximum error is approximately up to the order of 10^{-3}. Once again, our numerical method performed well as compared to those available in the literature.[28,34]

Problem 4. Aggregation and breakage.

Aggregation and breakage are two important processes in a crystallization process. The initial distribution is taken as

$$n(0,x) = \frac{3N_0^2}{V_0}x^2 \exp\left(-\frac{N_0 x^3}{V_0}\right), \tag{40}$$

where, $N_0 = 1\ \mathrm{m}^{-3}$ and $V_0 = 0.001\ \mathrm{m}^3$. A constant kernel aggregation term, $\beta(x,\lambda) = \beta_0 = 1$, and a binary breakage kernel $a(x) = a_0 x^3$ with $a_0 = 1$ are chosen. Moreover, a uniform daughter distribution given by Eq. 38 is considered. The analytical solution is given by

$$n(t,x) = 3x^2\frac{N_0^2}{V_0}\varphi^2(\tau)\exp\left(-\frac{N_0}{V_0}x^3\varphi(\tau)\right), \tag{41}$$

where

$$\varphi(T) = \varphi(\infty)\left[\frac{1+\varphi(\infty)\tanh(\varphi(\infty)\tau/2)}{\varphi(\infty)+\tanh(\varphi(\infty)\tau/2)}\right],$$
$$\varphi(\infty) = \frac{(2a_0V_0/C_0)^{1/2}}{N_0} \tag{42}$$

and $\tau = \beta_0 N_0 t$. The numerical results are shown in Figure 9. The moments of the numerical scheme are in good agreement with those obtained from the analytical solution. The figure also shows that the maximum relative error is of the order 10^{-3}. The error in μ_3 is of the order 10^{-16} and is therefore not displayed. Moreover, the maximum relative error in $\mu_5(t)$ is much lesser than published ones.[28,34]

Problem 5. Nucleation, growth, aggregation, and breakage.

Suppose that the stiff nucleation takes place at a minimum crystal size ($x_0 = 0$) as a function of time[7]

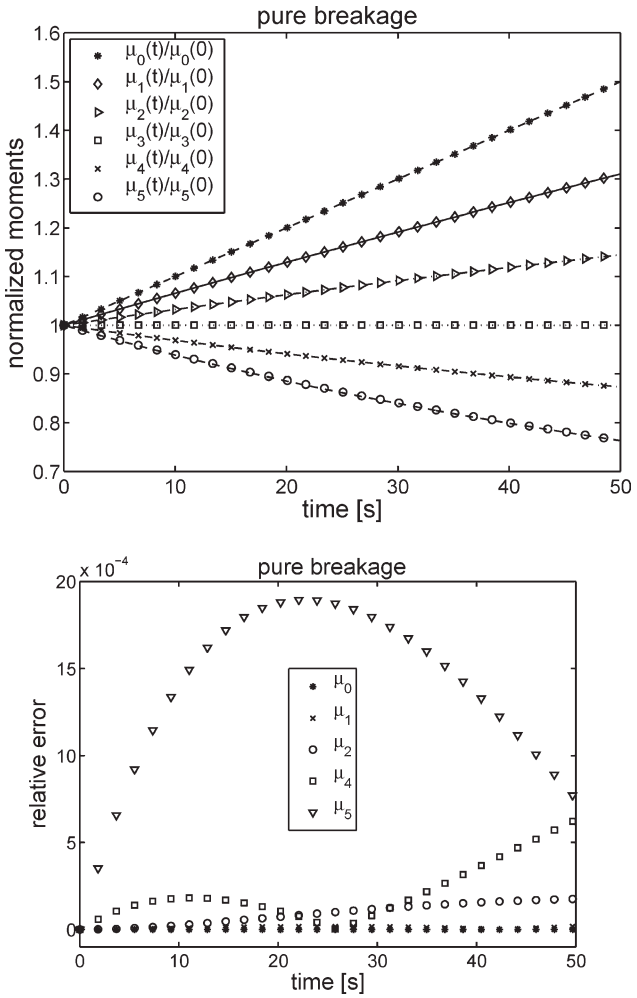

Figure 8. Problem 3: pure breakage (lines: exact solution, symbols: QMOM solution).

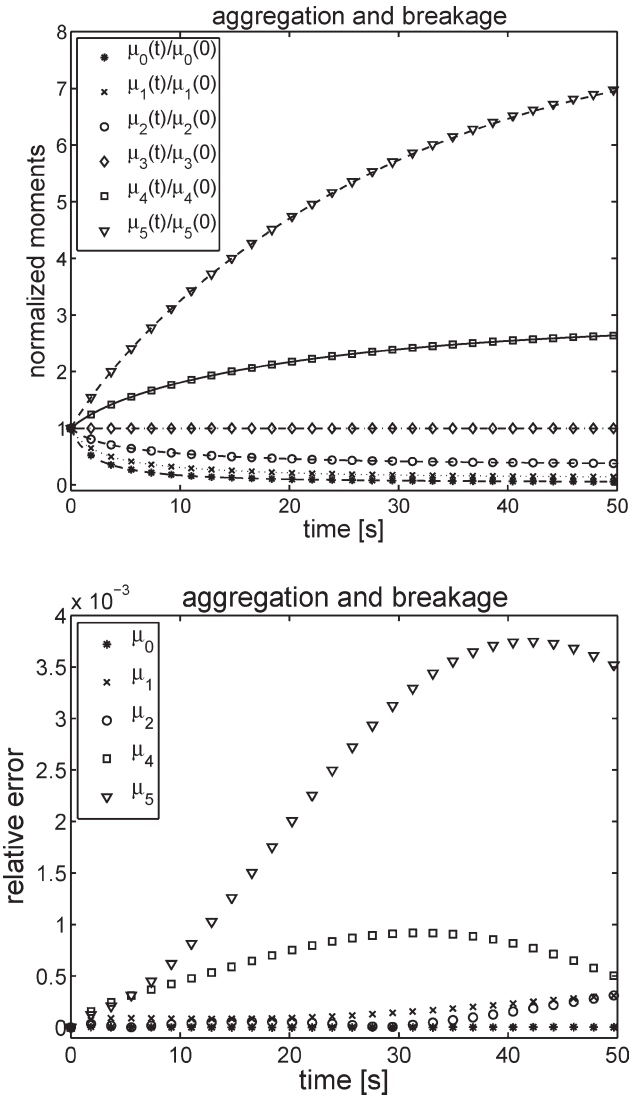

Figure 9. Problem 4: aggregation and breakage (lines: exact solution, symbols: QMOM solution).

$$n(t,0) = 100 + 10^6 \exp(-10^4(t-0.215)^2). \quad (43)$$

The particle size and time ranges are $0 \le x \le 2.0$ m and $0 \le t \le 0.5$ s, respectively. The square step initial condition for the number density is given as

$$n(0,x) = \begin{cases} 100 & \text{for } 0.4 \le x \le 0.6, \\ 0.01 & \text{elsewhere.} \end{cases} \quad (44)$$

Here, we consider constant growth rate with $G = 1.0$ m/s. The analytical solution for only growth and nucleation is given as[7]

$$n(t,x) = \begin{cases} 100 + 10^6 \exp(-10^4((Gt-x)-0.215)^2) & \text{for } 0.0 \le x \le Gt, \\ 100 & \text{for } 0.4 \le x - Gt \le 0.6, \\ 0.01 & \text{elsewhere.} \end{cases} \quad (45)$$

In this solution, a square step discontinuous shock along with a narrow wave, originated due to nucleation, move along the propagation path line, $x = x_0 + Gt$. The aggregation and breakage rates are taken as $\beta = 1.5 \times 10^{-5}$, $a(x) = x^6$, and $b(x|\lambda)$ is the same as given by Eq. 38.

The numerical results are shown in Figure 10. The analytical solutions are represented by lines for pure growth and nucleation problem, while symbols are used for the QMOM solutions. In the second plot, lines are used for FVS solutions. The numerical results of QMOM are in good agreement with the analytical and FVS solutions.

Conclusions

An alternative QMOM technique was proposed for solving batch crystallization models describing crystals nucleation, size-dependent growth, aggregation, breakage, and dissolution of small nuclei below certain critical size. In this technique, orthogonal polynomials, obtained from the lower order moments, were used to find the quadrature points and

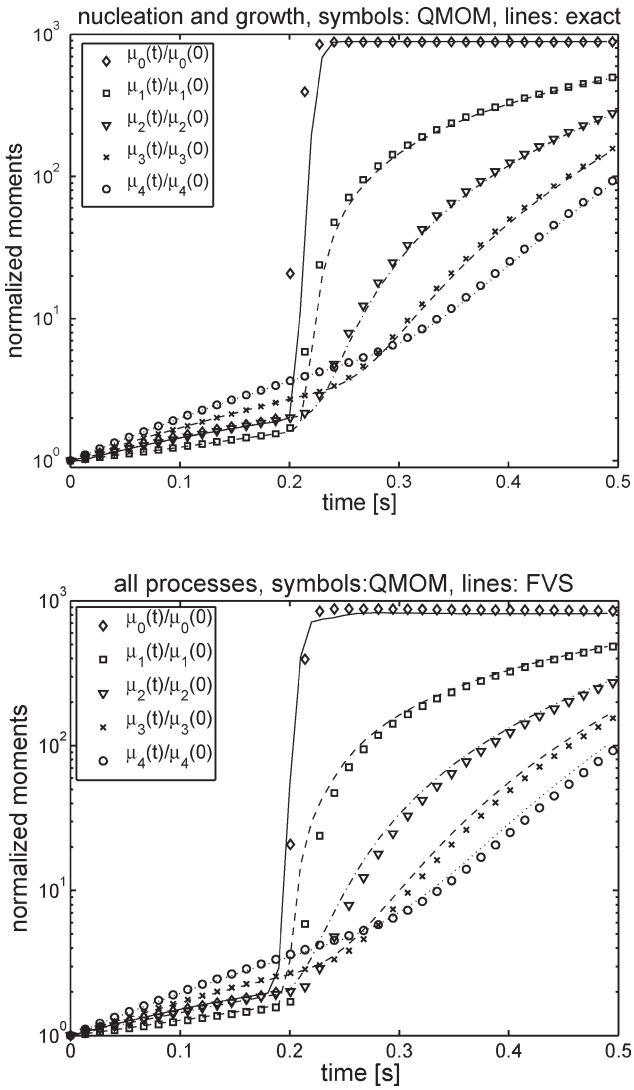

Figure 10. Problem 5: growth, nucleation, aggregation, and breakage processes.

weights. In this study, a third order orthogonal polynomial, utilizing first six moments, was selected. The required number of moments increases as the order of polynomial increases. However, the method has no restriction on the number of moments for any chosen polynomial, and is therefore capable to calculate all the moments required in a certain particulate process. The method is efficient due to the available analytical expression of orthogonal polynomial. Several numerical test cases with different combinations of processes were considered in this manuscript. The numerical results of the QMOM were validated against the analytical solutions, available results in the literature, and the results of a finite volume scheme. The results indicate that our method has a capability to accurately predict the moments evolutions in all test problems. In contrast to the method of classes and finite volume schemes, which preserve only two moments, our method has a capability to preserve all the moments involved in the quadrature approximation with less amount of errors. The main disadvantage of QMOM method is that the complete PSD is not directly available. However, in some cases the PSD is not needed and the lower order moments are sufficient to recover the valuable quantities. In addition, it is possible in some application to reconstruct the PSD by tracking only a few lower order moments.

Acknowledgments

A partial support by Higher Education Commission of Pakistan (HEC) is gratefully acknowledged.

Literature Cited

1. Hulburt HM, Katz S. Some problems in particle technology. *Chem Eng Sci*. 1964;19:555–574.
2. Randolph A, Larson MA. *Theory of Particulate Processes*, 2nd ed. San Diego, CA, Academic Press, Inc., 1988.
3. Barrett JC, Jheeta JS. Improving the accuracy of the moments method for solving the aerosol general dynamic equation. *J Aerosol Sci*. 1996;27:1135–1142.
4. Madras G, McCoy BJ. Reversible crystal growth-dissolution and aggregation breakage: numerical and moment solutions for population balance equations. *Powder Technol*. 2004;143–144:297–307.
5. Marchisio DL, Vigil RD, Fox RO. Quadrature method of moments for aggregation-breakage processes. *J Colloid Interface Sci*. 2003;258:322–334.
6. McGraw R, Nemesur S, Schwartz SE. Description of aerosol dynamics by the quadrature method of moments. *Aerosol Sci Tech*. 1997;27:255–265.
7. Lim YI, Lann J-ML, Meyer LM, Joulia L, Lee G, Yoon ES. On the solution of population balance equation (PBE) with accurate front tracking method in practical crystallization processes. *Chem Eng Sci*. 2002;57:3715–3732.
8. Qamar S, Warnecke G, Elsner MP. On the solution of population balances for nucleation, growth, aggregation and breakage processes. *Chem Eng Sci*. 2009;64:2088–2095.
9. Rawlings JB, Witkowski WR, Eaton JW. Modelling and control of crystallizers. *Powder Technol*. 1992;69:3–9.
10. Smith M, Matsoukas T. Constant-number Monte Carlo simulation of population balances. *Chem Eng Sci*. 1998;53:1777–1786.
11. Tandon P, Rosner DE. Monte Carlo simulation of particle aggregation and simultaneous restructuring. *J Coll Int Sci*. 1999;213:273–286.
12. Kumar S, Ramkrishna D. On the solution of population balance equations by discretization-I. A fixed pivot technique. *Chem Eng Sci*. 1996;51:1311–1332.
13. Dorao CA, Jakobsen HA. Numerical calculation of the moments of the population balance equation. *J Comput Appl Math*. 2006;196: 619–633.
14. Dorao CA, Jakobsen HA. A least squares method for the solution of population balance problems. *Comput Chem Eng*. 2006;30:535–547.
15. Dorao CA, Lucas D, Jakobsen HA. Prediction of the evolution of the dispersed phase in bubbly flow problems. *Appl Math Model*. 2008;32:1813–1833.
16. Gunawan R, Fusman I, Braatz RD. High resolution algorithms for multidimensional population balance equations. *AIChE J*. 2004;50: 2738–2749.
17. Qamar S, Elsner MP, Angelov I, Warnecke G, Seidel-Morgenstern A. A comparative study of high resolution schemes for solving population balances in crystallization. *Comp Chem Eng*. 2006;30:1119–1131.
18. McGraw R. Properties and evolution of Aerosol with size distributions having identical moments. *J Aerosol Sci*. 1998;29:761–772.
19. Marchisio DL, Pikturna JT, Fox RO, Vigil RD, Barresi AA. Quadrature method of moments for population balance equations. *AIChE J*. 2003;49:1266–1276.
20. John V, Angelov I, Öncül AA, Thévenin D. Technique for the reconstruction of a distribution from a finite number of its moments. *Chem Eng Sci*. 2007;62:2890–2904.
21. Grosch R, Briesen H, Marquardt W, Wulkow M. Generalization and numerical investigation of QMOM. *AIChE J*. 2006;53:207–227.
22. Diemer RB, Olson JH. A moment methodology for coagulation and breakage problems: Part I—analytical solution of the steady-state population balance. *Chem Eng Sci*. 2002;57:2193–2209.
23. Gordon RG. Error bounds in equilibrium statistical mechanics. *J Math Phys*. 1968;9:655–663.
24. Rosner DE, Pyykonen JJ. Bivariate moment simulation of coagulating and sintering nanoparticles in flames. *AIChE J*. 2002;48:476–491.
25. Wright DL, McGraw R, Rosner DE. Bivariate extension of the quadrature method of moments for modeling simultaneous coagulation and sintering of particle populations. *J Coll Int Sci*. 2001;236:242–251.
26. Barrett JC, Webb NA. A comparison of some approximate methods for solving the aerosol general dynamic equation. *J Aerosol Sci*. 1998;29:31–39.
27. Fan R, Marchisio DL, Fox RO. Application of the direct quadrature method of moments to polydisperse gas-solid fluidized beds. *Powder Technol*. 2004;139:7–20.
28. Su J, Gu Z, Li Y, Feng S, Xu XY. An adaptive direct quadrature method of moment for population balance equations. *AIChE*. 2008;54:2872–2887.
29. Gimbun J, Nagy ZK, Rielly CD. Simultaneous quadrature method of moments for the solution of population balance equations, using a differential algebraic equation frameworks. *Ind Eng Chem Res*. 2009;48:7798–7812.
30. Diemer RB, Ehrman SH. Pipeline agglomerator design as a model test case. *Powder Technol*. 2005;156:129–145.
31. Press WH, Teukolsky SA, Vetterling WT, Flannery BP. *Numerical Recipes: the Art of Scientific Computing*, 3rd ed. New York: Cambridge University Press, 2007.
32. Qamar S, Mukhtar S, Seidel-Morgenstern A, Elsner MP. An efficient numerical technique for solving one-dimensional batch crystallization models with size-dependent growth rates. *Chem Eng Sci*. 2009;64:3659–3667.
33. Miller SM, Rawlings JB. Model identification and quality control strategies for batch cooling crystallizers. *AIChE J*. 1994;40:1312–1327.
34. Su J, Gu Z, Li Y, Feng S, Xu XY. Solution of population balance equation using quadrature method of moments with an adjustable factor. *Chem Eng Sci*. 2007;62:5897–5911.
35. Scott WT. Analytic studies of cloud droplet coalescence I. *J Atmos Sci*. 1968;25:54–65.
36. Smit DJ, Hounslow MJ, Paterson WR. Aggregation and gelation. I. Analytical solutions for CST and batch operation. *Chem Eng Sci*. 1994;49:1025–1035.
37. Ziff RM, McGrady ED. The kinetics of cluster fragmentation and depolymerisation. *J Phys A Math Gen*. 1985;18:3027–3037.

Manuscript received Nov. 10, 2009, and revision received Feb. 8, 2010.